Send Orders for Reprints to reprints@benthamscience.net

RESEARCH ARTICLE

New Insights on the UV/TiO_2 Photocatalytic Treatment of Thiomersal and its 2-Sulfobenzoic Acid Product

Emmanuel M. de la Fournière[a], Jorge M. Meichtry[a,b], Graciela S. Custo[a], Eduardo A. Gautier[a], Marta I. Litter[c]*

[a]*Comisión Nacional de Energía Atómica, Av. Gral. Paz 1499, 1650 San Martín, Prov. de Buenos Aires, Argentina;* [b]*Centro de Tecnologías Químicas, Facultad Regional Buenos Aires, Universidad Tecnológica Nacional, Medrano 951, 1425 Buenos Aires, Argentina;* [c]*Instituto de Investigación e Ingeniería Ambiental –IIIA, UNSAM, CONICET, 3iA, Universidad de San Martín, Campus Miguelete, 25 de Mayo y Francia, 1650, San Martín, Prov. de Buenos Aires, Argentina*

ARTICLE HISTORY

Received:
Revised:
Accepted:

DOI:

Abstract:

***Background*:** Thiomersal (TM), a complex between 2-mercaptobenzoic acid (2-MBA) and ethylmercury ($C_2H_5Hg^+$), is an antimicrobial preservative used in immunological, ophthalmic, cosmetic products, and vaccines.

***Objective*:** TM has been treated by UV/TiO_2 photocatalysis in the presence or absence of oxygen at acidic pH. $C_2H_5Hg^+$, 2-MBA, and 2-sulfobenzoic acid (2-SBA) were found as products. A 2-SBA photocatalytic treatment was undertaken to study sulfur evolution.

Methods: Photocatalytic runs were performed using a UVA lamp (λ_{max} = 352 nm), open to air or under N_2. A suspension of the corresponding TM or 2-SBA salt and TiO_2 was prepared, and pH was adjusted. Suspensions were stirred in the dark for 30 min and then irradiated. TM, 2-MBA, 2-SBA, and $C_2H_5Hg^+$ were quantified by HPLC, sulfur by TXRF, and the deposits on the photocatalyst were analyzed by chemical reactions. The mineralization degree was followed by TOC. Sulfate was determined using $BaCl_2$ at 580 nm.

***Results*:** Photocatalytic destruction of TM and total $C_2H_5Hg^+$ was complete under N_2 and air, but TM degradation was much faster in air. The evolution of TM and the products followed a pseudo-first order kinetics.

Conclusion: TiO_2-photocatalytic degradation is a suitable technique for the treatment of TM and its degradation products. In contrast to other organomercurial compounds, TM degradation is faster in the presence of O_2, indicating that the oxidative mechanism is the preferred pathway. A significant TM mineralization (> 60%, NPOC and total S) was obtained. TM was more easily degraded than 2-SBA. Sulfate was the final product.

Keywords: Heterogeneous photocatalysis, Thimerosal, Ethylmercury 2-Mercaptobenzoic acid, 2-Sulfobenzoic acid, Titanium dioxide.

1. INTRODUCTION

Mercury is an extremely hazardous and persistent contaminant, which can cause several health effects in humans; polluted waters are the main exposure source with contamination from anthropogenic and natural processes [1-5].

Thiomersal (thimerosal, mercury((o-carboxyphenyl)thio)ethyl sodium), TM), a complex between 2-mercaptobenzoic acid (2-MBA, thiosalicylic acid) and ethylmercury ($C_2H_5Hg^+$), is an antimicrobial preservative and stabilizer used in immunological, ophthalmic, and cosmetic products, and mainly in human and veterinary vaccines [6-11]. Yearly, loss of thousands of vaccines occurs due to expiration, loss of cold chain and overstock, and safe disposal of expired vaccines containing thimerosal has become a high priority.

The chemical structure of TM is presented in Fig. 1.

* Address correspondence to this author at Instituto de Investigación e Ingeniería Ambiental–IIIA, UNSAM, CONICET, 3iA, San Martin, Buenos Aires Prov., Argentina; Tel: 5491130132815; e-mail: marta.litter@gmail.com.

2665-976X /19 $58.00+.00

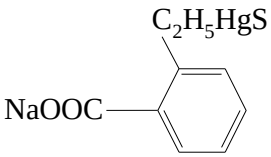

Fig. 1. Chemical structure of thiomersal.

TM is in equilibrium with the sodium salt of 2-MBA and $C_2H_5Hg^+$ (Eq. (1)) and TM is metabolized in the human body to 2-MBA and ethyl mercury (a very toxic pollutant) [12].

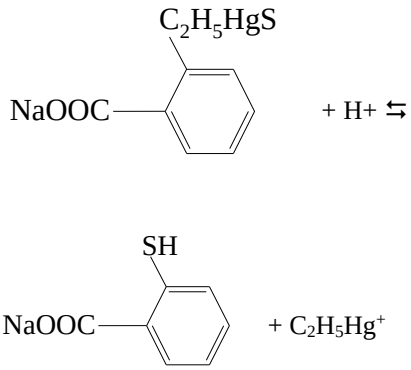

(1)

In 1999, TM was suspected by the US Public Health Service and the American Academy of Pediatrics to be toxic in accumulated doses of ethylmercury in vaccinated infants [13]. However, in 2006, the WHO concluded that there was no relationship between vaccines containing TM and neurological troubles in vaccinated children [14]. Nowadays, the controversy is still open [15-21]. Ethylmercury, generated from TM, is assumed to pass through the blood-brain barrier, resulting in Hg accumulating in the brain [21], where it may cause oxidative stress [22], and alter brain autoantibodies formation [20]. The WHO limit for inorganic Hg in drinking water is 0.006 mg L^{-1} [23].

Because TM is likely to be present in waste streams from hospitals, clinical laboratories, and pharmaceutical industries, its degradation is of environmental concern. Spontaneous oxidation [24], biodegradation by a mercury- resistant strain of *Pseudomonas putida* [25], carbon adsorption processes [9], and photodecomposition using UV irradiation of high energy [26-28] have been evaluated for TM treatment. In all cases, remediation processes require special conditions, suppose high costs, or do not resolve the problem as the pollutant is only transferred to another phase and not degraded to less toxic products. Heterogeneous photocatalysis emerges as a possible remediation technology. Previous works were made on the TiO_2 photocatalytic inorganic mercury(II) reduction under UVA light and even under solar light [5, 29-34]. The TiO_2 photocatalytic treatment of organomercurial compounds is scarce, being phenylmercury [35,36], methylmercury [37,38], and ethylmercury [39] the only studied systems reported in the literature. In all cases, and depending on the conditions, Hg, HgO, and/or calomel (Hg_2Cl_2) were deposited on the photocatalyst.

Only two studies report the photocatalytic degradation of TM. Yepsen et al. [11] studied TiO_2 heterogeneous photocatalysis (pH 2 and 0.2 g L^{-1} TiO_2, N_2 bubbling) under UV-A in the presence of formic acid as a sacrificial agent. Dissolved Hg(II), Hg(0), salicylic acid, and other intermediate oxidation products were found; all organic compounds were finally mineralized. Miranda-Andrades et al. [40] performed the photodegradation of TM under visible light using graphene quantum dots as catalysts, which converted TM into ethylmercury and then to Hg^{2+}; this species was further reduced to Hg(0) with $SnCl_2$.

In contrast, the treatment of sulfur pollutants by heterogeneous photocatalysis has been widely reported (mainly in aqueous systems). Several years ago, Herrmann [41] reviewed the subject and reported that, according to previous papers [42-44], compounds containing sulfur atoms are mineralized into sulfate ions. For example, Kerzhentsev et al. [43] studied the degradation of the insecticide fenitrothion using TiO_2 aqueous suspensions under irradiation at $\lambda > 340$ nm, achieving the mineralization into CO_2, $H_2PO_4^-$, SO_4^{2-} and NO_3^-. Similarly, Pelizzetti et al. [44] studied the degradation of the herbicide bentazon by AM1 simulated sunlight in aqueous suspensions of TiO_2, achieving the near quantitative recovery of SO_4^{2-} ions and CO_2. Hun et al. [45] examined the UVA photocatalytic degradation of sulfamethoxazole (SMX) and related sulfonamide antimicrobial agents in TiO_2 aqueous suspensions. Elmolla and Chaudhuri [46] analyzed the heterogeneous photocatalytic degradation of amoxicillin, ampicillin, and cloxacillin, three antibiotics containing C-S-C bounds with H_2O_2 addition; in all cases, sulfate was the final degradation product containing S. Ampicillin was also treated by heterogeneous photocatalysis in another work, finding that the sulfur group was degraded to SO_4^{2-} as final product [47]. The TiO_2 photocatalytic degradation of the antibiotic dicloxacillin achieved a complete removal after 120 min, with 95% mineralization after 480 min [48]. TiO_2 photocatalysis of β-lactam oxacillin in water was also studied [49], with 100% degradation after 45 min, and 90% mineralization after 135 min. TiO_2 supported over SBA-15 mesoporous molecular sieves has been tested for the photocatalytic degradation of dimethoate; PO_4^{3-}, SO_4^{2-}, NO_3^-, CO_2 and H_2O were the final mineralization products [50]. Bian et al. [51] studied the photocatalytic degradation of sodium isobutyl xanthate (SIBX) in aqueous solution, using nitrogen and cerium co-doping TiO_2-coated activated carbon, SIBX was first degraded to C_4H_9OH and CS_2, which was then transformed into CS_2OH, COS, and HS^-.

In conclusion, organic sulfur compounds can be easily degraded by photocatalytic processes, being the degradation initiated by the attack of h_{VB}^+ and $HO^\bullet$ (superoxide radical can be also involved) on the electron-rich S group, which is oxidized, ending in SO_4^{2-} as the final stable product; the formation of volatile S compounds cannot be completely ruled out.

Heterogeneous photocatalysis of S-containing compounds in the gas phase or organic solvents have been also studied, most using TiO_2 or modified TiO_2 as can be seen in references [52-63] and other works.

In this paper, the conditions to perform efficient heterogeneous photocatalysis to promote the degradation of TM and sulfobenzoic acid (2-SBA, one of the products of the TM photocatalytic degradation) have been studied. As far as these authors know, no references exist in the literature regarding the photocatalytic degradation of 2-SBA.

2. MATERIALS AND METHOD

2.1. Materials

TiO_2 was Evonik P25 Aeroxide (P25), used without further purification. TM ($C_9H_9HgNaO_2S$, purity > 97%) was Sigma, and C_2H_5HgCl (purity 95%), 2-SBA ($C_7H_6O_5S.xH_2O$, purity 95%) and 2-MBA ($C_7H_6O_2S$, purity 98%) were Alfa Aesar. All other reagents were at least of reagent grade and used without further purification. Solutions were prepared with Milli-Q water (resistivity = 18 MΩ.cm). Dilute NaOH solutions were used to adjust pH.

2.2. Photocatalytic experiments

Photocatalytic runs were carried out in a recirculating system previously described [39] (1.5 L min^{-1} flow rate, thermostatted at 25 ºC). A black-light tubular UV lamp (FLBLB, Toshiba Electric, 15 W, 300 < λ/nm < 400, 100% maximum emission at 352 nm) was used as source of illumination. Actinometric measurements, performed by the ferrioxalate method, indicated that the photon flux per unit of volume ($q^0_{n,p}/V$) was 2.87 μeinstein s^{-1} L^{-1}.

The reaction was conducted under a water-saturated N_2 stream bubbled in the suspension at 0.4 L min^{-1} throughout the experiment, or with the reactor open to air ([O_2] ≈ 2 mg L^{-1}). In all cases, a fresh solution (500 mL) of the corresponding salt was used (0.1 or 0.5 mM), the catalyst (1 g L^{-1}) was suspended in the solution, and the system was adjusted to the desired pH value (4 or 10); then, the suspension was ultrasonicated for 2 min. Before irradiation, suspensions were stirred in the dark for 30 min to assure substrate – surface equilibrium, a time frequently used in photocatalytic experiments over TiO_2. The extent of adsorption of mercury compounds onto TiO_2 under N_2 or in air was determined by measuring concentrations in the filtrate (see below) before and after stirring in the dark. Initial pH values of TM or 2-SBA solutions were measured in the suspension after equilibration in the dark, and pH was left to vary freely during the experiments. Samples were periodically withdrawn and filtered through 0.22 μm Millipore filters. At least, duplicated runs were carried out for each condition, averaging the results; however, in some cases, several runs were performed to assure reproducibility, especially in the presence of O_2. In all cases, the amount of the compound adsorbed in the dark was discounted to analyze only the effect of light on the photocatalytic transformation.

2.3. Analytical procedures

TM, 2-MBA, 2-SBA, and $C_2H_5Hg^+$ were quantified by HPLC. The chromatographic system consisted of an Alltech 301 HPLC Pump, a 100-μL loop, a Thermo C18 column (5 μm, 15 cm × 4.6 mm), and a Spectra SYSTEM UV1000 detector. A methanol/10 mM phosphate buffer (pH 6) solution (55:45) mobile phase at a flow rate of 0.4 mL min^{-1} was used. Detection was carried out at 250 nm. For total $C_2H_5Hg^+$ concentration ($C_2H_5Hg^+_T$, equal to the sum of TM plus free $C_2H_5Hg^+$) and mercury speciation in the filtrate, an HPLC method developed by the group was used [64]. The mobile phase was composed of CH_3OH–CH_3CN–5 mM NaH_2PO_4 (1:4:5) containing 0.1 mM 2-mercaptopropionic acid. A flow rate of 0.8 mL min^{-1} was employed, and analytical measurements were carried out at 220 nm. Within the experimental error, $C_2H_5Hg^+_T$ concentration measured by both HPLC techniques were identical. In all HPLC measurements, data acquisition was processed with Konikrom software.

Total sulfur analysis was carried out using an X-ray fluorescence system with total reflection geometry (TXRF). The spectrometer consists of a Seifert X-ray generator, and the total reflection module was fitted with a cut-off-filtered radiation from a fine focus diffraction molybdenum anode X-ray tube. The detection and data acquisition system comprised an 80 mm^2 Si(Li) detector with 166 eV FWHM for 5.9 keV, an 8 μm thick Be window, an Ortec 672 fast spectroscopy amplifier, and an ADC Nucleus PCA2. Excitation conditions were 50 kV and 30 mA in all cases. The acquisition time for each spectrum was 300 s.

Absorbance measurements were done with an HP 8453 diode-array UV-Vis spectrophotometer, using 1 cm pathlength quartz cells. Dissolved oxygen (DO) measurements were performed with a Hach SensIon 156 dissolved oxygen meter (detection limit, DL, 0.05 mg O_2 L^{-1}). The deposits on the recovered photocatalysts were analyzed by chemical reactions for the identification of different products. A gray deposit, soluble in concentrated nitric acid, corresponded to metallic Hg (Hg(0)) [65,66], and was observed just after 60 min reaction, either under N_2 or in air. Treatment of the deposit with 2.5 M KI, giving a filtrate absorbing at 323 nm, indicated HgO [67,68].

The mineralization degree was followed by total organic carbon (TOC) analysis, using a Shimadzu 5000A TOC analyzer in the non-purgeable organic carbon mode (NPOC). Sulfate in solution was determined by the turbidimetric method using $BaCl_2$ at 580 nm (DL = 3 mg L^{-1}) [69]. For the analysis in the deposits, the TiO_2 separated by filtration was resuspended in pure water and stirred in the dark for 5 min; then, this suspension was filtered and the filtrate was analyzed.

3. RESULTS

3.1 Reaction in the dark and in the absence of photocatalyst

Preliminary assays in this work showed that no significant TM degradation took place in the dark and that UV photolysis of TM did not take place in the 300-400 nm range employed, as expected from the lack of TM absorption in this range (see Fig. S1 in the supporting information section (SI)). This is in agreement with the results of Yepsen et al. [11], who reported for TM two absorption bands in the UV-C range (233 and 263 nm), and no photolysis of the compound when using a UV-A lamp in the absence of a photocatalyst. Besides, references [26-28] indicate that high energy UV irradiation is needed for an efficient TM photolysis. Besides, in the presence of TiO_2, UV irradiation emitted by the lamp would be largely absorbed by the photocatalyst, as indicated in our previous study on $C_2H_5Hg^+$ [39].

3.2. Photocatalytic removal of TM and its degradation products

Photocatalytic experiments were mostly performed in suspensions containing 0.5 mM TM at pH 4 and 1 g L^{-1} TiO_2

at 25 ºC under N_2 bubbling or with the reactor open to air. At t = 0 min, TM is partially dissociated into 2-MBA and $C_2H_5Hg^+$ ([2-MBA] = 0.003 mM and $[C_2H_5Hg^+]$ = 0.005 mM) and, after the adsorption equilibrium was reached (30 min stirring in the dark), TM concentration decreased from the initial value ($[TM]_0$ = 0.500 mM) to an equilibrium concentration ($[TM]_e$ = 0.46 mM). The adsorption of TM over TiO_2 at pH 4 is favored due to electrostatic attraction, as at this pH the compound is negatively charged (pK_a 3.05 [70]), and the P25 surface is positive (pH of PZC 6-7 [71]). Therefore, $[TM]_e$ will be considered the initial concentration for the photocatalytic experiments, and it is almost identical to the equilibrium concentration of $C_2H_5Hg^+$ ($[C_2H_5Hg^+]_e$ = 0.47 mM) under the same initial experimental conditions (0.50 mM) [39].

Fig. 2 shows the evolution of TM and total ethylmercury ($[C_2H_5Hg^+_T] = [TM] + [C_2H_5Hg^+]$, considering that $C_2H_5Hg^+$ can be produced by the hydrolysis of TM (see Fig. 1 and Eq. (1)). Concentrations are normalized with respect to $[TM]_e$ and $[C_2H_5Hg^+_T]_e$. As shown, photocatalytic destruction of TM and $C_2H_5Hg^+_T$ under N_2 is complete at 240 min; TM reaction is faster under air, being almost completely degraded at around 60 min; in contrast, for $C_2H_5Hg^+_T$ complete depletion, 240 min irradiation is required. It should be mentioned that as TM photocatalytic degradation proceeds, the pH of the system slightly decreases (from 4 to 3.5 at 240 min), either under N_2 or air.

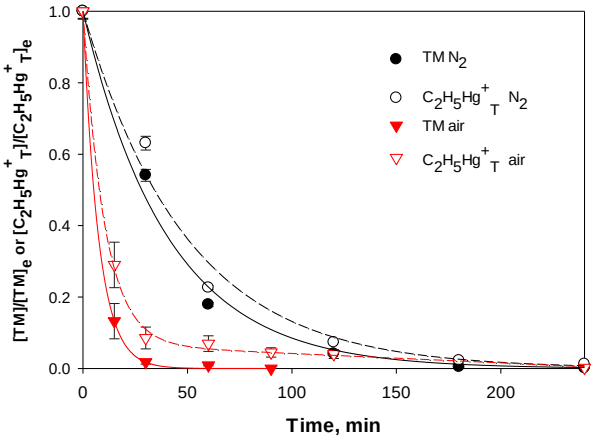

Fig. 2. Evolution profiles of TM and $C_2H_5Hg^+_T$ concentrations normalized with respect to $[TM]_e$ and $[C_2H_5Hg^+_T]_e$ during TM photocatalytic runs under N_2 or air. Conditions: $[TM]_0$ = 0.5 mM, pH_0 4, $[TiO_2]$ = 1 g L^{-1}, T = 25 ºC, $q^0_{n,p}/V$ = 2.87 μeinstein s^{-1} L^{-1}. N_2: Q_{N2} = 0.4 mg L^{-1} ($[O_2]$ < 0.05 mg L^{-1}); air: reactor open to air ($[O_2]$ ≈ 2 mg L^{-1}). Solid lines are the fittings of [TM] evolution to a pseudo-first order kinetics (Eq. (S3)); short dashed lines represents $C_2H_5Hg^+_T$ evolution, adjusted to a pseudo-first order for the case of the reaction under N_2 and to a pseudo-first order combined with a zero-order kinetics for the case of the reaction in air (see text).

As it can be appreciated, TM and $C_2H_5Hg^+_T$ curves followed a similar behavior, with a decreasing degradation rate as the reaction proceeds, indicating that: 1) their concentration plays a role in the photocatalytic degradation rate, and 2) that TiO_2 deactivation, caused by Hg(0) deposition [29, 39,72], is taking place.

As intermediates of the organic moiety of TM, $C_2H_5Hg^+$, 2-MBA, and 2-SBA have been identified and quantified by HPLC. TM and $C_2H_5Hg^+$ are the main toxic compounds. The evolution profiles of $C_2H_5Hg^+$, 2-MBA, and 2-SBA concentrations and of an aromatic (due to the 250 nm detection wavelength used), non-identified intermediate (UI) during the TM photocatalytic experiment under N_2 are shown in Fig. 3 together with the decay of [TM]. Hg^{2+} ($[Hg^{2+}] \approx 0.05$ mM), produced by the photocatalytic degradation of $C_2H_5Hg^+$ [39] was measured. Consequently, all Hg not found as TM, $C_2H_5Hg^+$, or Hg(II) would be deposited over the photocatalyst as Hg(0) (see below). Other non-identified compounds were also detected; these compounds are probably aromatics and could be salicylic and dithiosalicylic acids, as found by Yepsen et al. 2015 [11]. As said before, due to partial dissociation of TM into 2-MBA and $C_2H_5Hg^+$, at t = 0 min, the 2-MBA concentration is 0.003 mM and that of $C_2H_5Hg^+$ is 0.005 mM. As it can be appreciated, both 2-MBA and $C_2H_5Hg^+$ reached their maximal concentration (0.11 and 0.05 mM, respectively) at 30 min, followed by a rather fast decrease. At longer times, the degradation rates decrease, and those compounds can be still detected after 240 min (0.008 and 0.005 mM for 2-MBA and $C_2H_5Hg^+$, respectively). The maximum 2-SBA concentration can be viewed at around 60 min, followed by a slow decrease at longer times. A similar behavior is observed for UI, which showed a maximum concentration at around t = 120 min; both 2-SBA and UI are still present in important concentrations after 240 min.

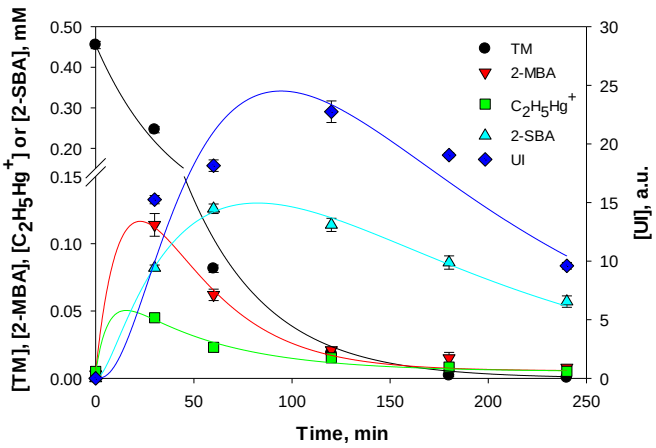

Fig. 3. Evolution of the concentration of TM and of intermediates formed during the photocatalytic reaction under N_2 bubbling. Conditions of Fig. 2. Lines represent the fittings of [TM], $[C_2H_5Hg^+]$, [2-MBA], [2-SBA] and [UI] to Eqs. (S3), (S6), (S7), (S9), and (S11), respectively. Note: for [UI], absorbance data reported by the equipment are plotted.

In addition, it should be emphasized that, under N_2, at t = 240 min, $C_2H_5Hg^+$ can be still detected (see Fig. 2 and Fig. 3 below, $[C_2H_5Hg^+]$ = 0.005 mM), despite TM was almost completely degraded at t = 120 min ([TM] = 0.019 mM). Further $C_2H_5Hg^+$ generation was stopped ($[C_2H_5Hg^+]$ = 0.015 mM at t = 120 min). From t = 120 up to 240 min, only 0.029 mM of $C_2H_5Hg^+$ (considering that 0.019 mM of TM were completely transformed into $C_2H_5Hg^+$, and 0.015 mM corresponds to $C_2H_5Hg^+$) were degraded; in contrast, when starting from pure $C_2H_5Hg^+$, under almost identical

conditions, 0.16 mM $C_2H_5Hg^+$ were degraded in less than 15 min, and 0.50 mM where degraded in 60 min [39]. This indicates that, when TM is degraded, a strong inhibition on the $C_2H_5Hg^+$ photocatalytic degradation takes place, which can be attributed to TiO_2 deactivation, and to the competition between $C_2H_5Hg^+$ and other intermediates for the photocatalyst active sites.

The explanation for the pseudo-first order decay for $C_2H_5Hg^+{}_T$ under N_2 ($k = 20 \pm 2 \times 10^{-3}$ min^{-1}, $R^2 = 0.98$) is that both TM and $C_2H_5Hg^+$ adjust to a pseudo-first order kinetics. In contrast, $C_2H_5Hg^+{}_T$ in air follows a pseudo-first order combined with a zero order kinetics probably because TM follows a first order and $C_2H_5Hg^+$ follows a first order plus a zero order behavior ($k = 98 \pm 7 \times 10^{-3}$ min^{-1}, $k = 12 \pm 6 \times 10^{-5}$ mM min^{-1}, $R^2 = 0.998$), i.e., $C_2H_5Hg^+{}_T$ follows a similar behavior as TM + $C_2H_5Hg^+$.

Fig. 4 shows the evolution of intermediate species during the photocatalytic reaction of TM under the same conditions of Fig. 2 with the reactor open to air.

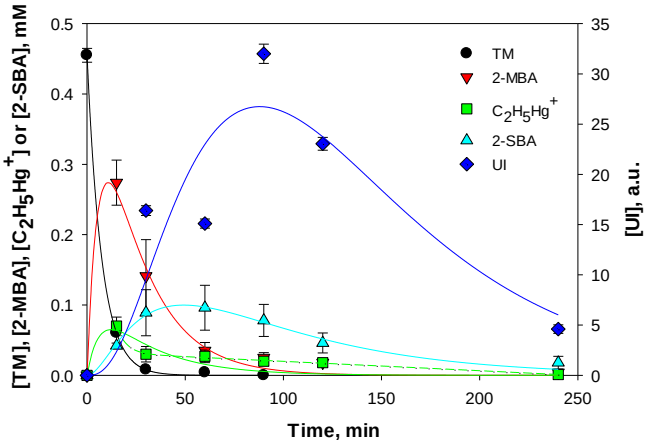

Fig. 4. Evolution of the concentration of TM and of intermediates formed during the photocatalytic reaction of TM with the reactor open to air. Conditions of Fig. 2, $[O_2] \approx 2$ mg L^{-1}. Solid lines represent the fittings of [TM], [$C_2H_5Hg^+$], [2-MBA], [2-SBA] and [UI] to Eqs. (S3), (S6), (S7), (S9), and (S11), respectively; the dashed line represents the fitting of $C_2H_5Hg^+$ for $t \geq 15$ min to a mixed, exponential plus zero order decay.

Profiles of Fig. 4 follow a similar behavior as those under N_2. TM is almost completely degraded at t = 60 min, and $C_2H_5Hg^+$ is within the DL at t = 240 min (Figs. 2 and 4), indicating that the reaction is more efficient under these conditions, contrarily to $C_2H_5Hg^+$ photocatalytic degradation, which was faster in the absence of O_2 [46]. This reinforces the strong inhibition on the $C_2H_5Hg^+$ photocatalytic degradation, as it was explained for the system under N_2. Hg^{2+} ([Hg^{2+}] ≈ 0.05 mM) is produced. As it can be appreciated, both 2-MBA and $C_2H_5Hg^+$ reached their maximal concentrations at 15 min (0.27 mM and 0.03 mM, respectively, values higher than those under N_2 and produced in a shorter time), followed by a rather fast decrease; these species can still be detected after 240 min at very low concentrations (0.004 and 0.001 mM for 2-MBA and $C_2H_5Hg^+$, respectively). On the other hand, the maximum 2-SBA concentration can be viewed at around 60 min, followed by a slow decrease at longer times. A similar behavior is observed for UI, produced here at higher concentrations than those observed under N_2. Both compounds are still present in important concentrations at 240 min.

Fig. 5 shows the evolution of [TM] and [2-SBA] normalized with respect to their equilibrium concentrations ($[TM]_e$ and $[2\text{-SBA}]_e$, respectively), for experiments starting from either TM or 2-SBA.

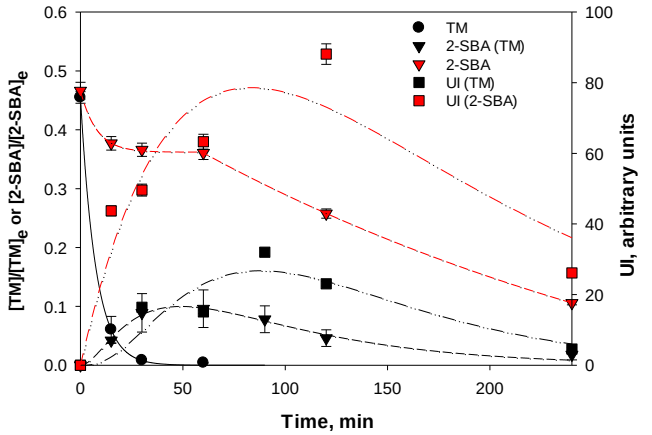

Fig. 5. Temporal profiles of normalized [TM] and [2-SBA] for experiments starting from either TM or 2-SBA; in the right y-axis, evolution of UI concentration (in arbitrary units). Conditions: $[TM]_0$ or $[2\text{-SBA}]_0$ = 0.5 mM, $[TiO_2]$ = 1 g L^{-1}, T = 25 ºC. pH$_0$ 4, reactor open to air, $q^0_{n,p}/V$ = 2.87 μeinstein s^{-1} L^{-1}. Black solid line: fitting of TM to Eq. (S3); black dashed line: fitting of 2-SBA generated from TM to Eq. (S9); black dashed-pointed line: fitting of UI from TM to Eq. (S11). Red lines for experiments starting from 2-SBA are explained in section 4.2. The line for UI generated from 2-SBA is only for visualization.

Fig. 5 indicates that, under the same experimental conditions, 2-SBA decays slower than TM; after an arrest in the degradation between 15 and 60 min of reaction, a continuous decrease can be observed, but the compound never disappears, in contrast with TM, which is totally depleted before 60 min. The UI intermediate formed from 2-SBA degradation presents a much higher concentration compared with that observed when starting from TM.

In Fig. 6, the NPOC and total S mineralization during the degradation of TM and 2-SBA with the reactor open to air are shown.

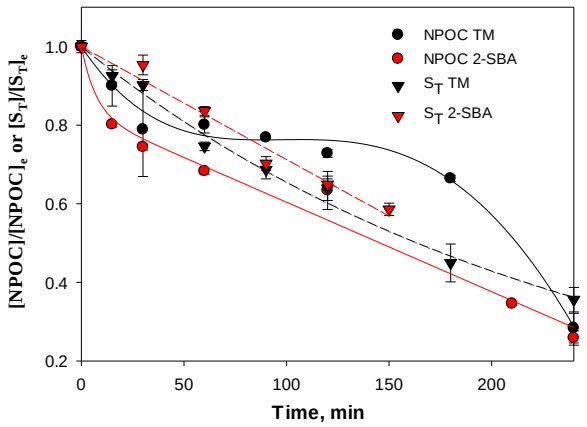

Fig. 6. Temporal profile of normalized NPOC and total sulphur (S_T) during the photocatalytic destruction of TM and SBA. Conditions: [TM] = [2-SBA] = 0.5 mM, [TiO_2] = 1 g L^{-1}, T = 25 ºC. pH_0 4, reactor open to air, $q^0_{n,p}/V$ = 2.87 μeinstein s^{-1} L^{-1}. Lines are only for visualization.

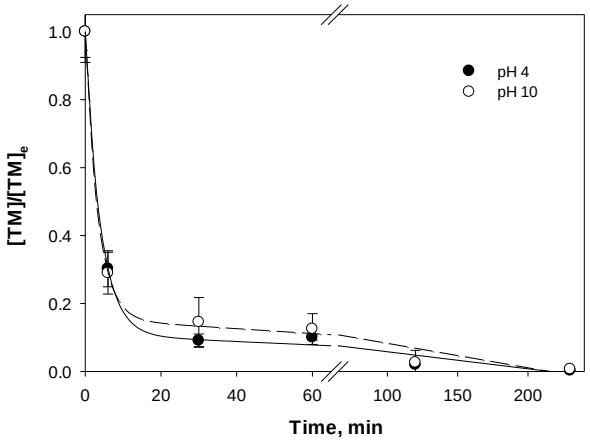

Fig. 7. Temporal profiles of TM normalized concentration during a photocatalytic run at two different pH_0. Conditions: [TM] = 0.1 mM, [TiO_2] = 1 g L^{-1}, T = 25 ºC, $q^0_{n,p}/V$ = 2.87 μeinstein s^{-1} L^{-1}, reactor open to air.

Fig. 6 shows that NPOC mineralization for TM up to 30 min is fast, in agreement with TM degradation (Fig. 2), reflecting that some mineralization occurs in the first degradation steps; then, the TM mineralization is arrested between 30 and 180 min, correspondingly with the degradation of 2-MBA into 2-SBA (as expected considering that no C mineralization occurs during this oxidation because both molecules have the same number of carbons), and of 2-SBA into UI. Then, once 2-SBA and UI degradation proceeds, C mineralization continues. NPOC mineralization for 2-SBA is initially fast ($t \leq 30$ min), and then continues with a slower decrease, similar to the behavior followed by 2-SBA (Fig. 5). No total mineralization is observed in any case, at least up to 240 min of reaction. On the other hand, S mineralization from TM decreases constantly during the whole process, indicating that S is continuously transformed into either sulfate, which is retained over the TiO_2 photocatalyst, and/or to volatile S compounds (i.e., SH_2 or organic sulfides of high vapor pressure).

Although sulfur mineralization is observed from the beginning when starting from either TM or 2-SBA, SO_4^{2-}, the final product of 2-SBA sulfur mineralization, was found to be present only after 120 min of reaction time. This also indicates that, even at a low rate, 2-SBA mineralization is taking place, simultaneously with TM, $C_2H_5Hg^+$, and 2-MBA photocatalytic degradation. A possible explanation of the high mineralization into sulfate is that it proceeds from sulfur volatile compounds, but this was not verified in this work.

3.3. Effect of pH on the photocatalytic TM removal and deposits found on the photocatalyst surface after the reaction

In Fig. 7, the results with the reactor open to air and [TM] = 0.1 mM, at two pH_0 values, 4 and 7, are shown; this concentration was chosen to see faster results. For both conditions, an adsorption degree of ≈ 50% of TM was measured.

As it can be observed, no significant differences were obtained at the two pH values, and a significant removal (≈ 70%) resulted after only 5 min of irradiation. For both conditions, TM degradation follows a fast, pseudo-first order kinetics, followed by a far slower, zero order one (k = 250 ± 30 × 10^{-3} min^{-1}, k_0 = 2.2 ± 0.8 × 10^{-5} mM min^{-1}, R^2 = 0.995 at pH 4; k = 300 ± 50 × 10^{-3} min^{-1}, k_0 = 4 ± 1 × 10^{-5} mM min^{-1}, R^2 = 0.991 at pH 10), probably because, at this lower TM concentration, the degradation of the formed by-products can compete more efficiently with TM for the TiO_2 active places, causing then the partial deactivation of the photocatalyst (i.e., by Hg(0) deposition and/or 2-SBA competition). An almost complete TM removal is obtained at 120 min; when compared with the experiment with 0.5 mM TM (Fig. 2), it is seen that the overall process is more efficient for the highest TM concentration (which disappears at 60 min). This contrasts with the behavior of other pollutants, e.g., Cr(VI) in the presence of citric acid [73] and other examples.

Deposits on the photocatalyst were observed at the end of the experiments. The compounds were identified by chemical methods, as indicated in the experimental section. Hg(0) was identified at pH 4.

The measurement of Hg(II) in solution at pH 4 indicated that the species reached the highest value of 0.05 mM after complete $C_2H_5Hg^+$ degradation. However, after 240 min of reaction, Hg(II) in solution was below the detection limit, which leads to the conclusion that the species was almost completely reduced to Hg(0); the appearance of the gray color on the photocatalyst confirms this assumption.

In contrast, at pH 10, no Hg(II) was detected in the solution. However, the analysis of the solids showed that a mixture of Hg(0) and HgO was formed, being these mercury species the only ones detected under these conditions. This indicates that, also at this pH, free Hg(II) is formed during TM photocatalytic degradation, which is fast transformed. As the analytical techniques used to measure Hg(0) and HgO are not very accurate, we cannot indicate how much of each species was formed at pH 10. Besides, Hg(0) is difficult to be measured because: 1) it is volatile; 2) it remains on the

photocatalyst surface, probably at a low concentration, which makes difficult the determination.

4. DISCUSSION

4.1. Mechanisms of TM photocatalytic removal

In order to propose a mechanism for TM photocatalytic removal, it is important to remember that the compound is in equilibrium with 2-MBA and $C_2H_5Hg^+$ (Eq. (1)). No reference was found in the literature regarding the value of the equilibrium constant of Eq. (1). However, the stability constants for the complex between 2-MBA and Hg(II) are high ($10^{25.7}$ [74]), while constants of methylmercury with thiol groups are in the range of 10^{11} – 10^{15} [75]; although no constants for ethylmercury were found, they might be considered similar to those of methylmercury.

It can be proposed that the decay of $C_2H_5Hg^+$, 2-MBA, 2-SBA, and UI formed in the photocatalytic reaction of TM can be modeled as consecutive steps. It can be hypothesized that two different radicals are formed from TM, as shown in Eqs. (2) and (3), this depending if the attack to TM takes place on the 2-MBA or on the $C_2H_5Hg^+$ moiety. This hypothesis is sustained by the experimental results of this work because both compounds have been detected. These reactions are followed by 2-MBA degradation to 2-SBA and of 2-SBA to UI, ending in SO_4^{2-}, CO_2, etc. A simplified reaction scheme is displayed by Eqs. (2) to (7).

$$TM \rightarrow C_2H_5Hg^+ + \text{2-MBA}^\bullet \qquad k_{1TMa} \quad (2)$$
$$TM \rightarrow C_2H_5Hg^\bullet + \text{2-MBA} \qquad k_{1TMb} \quad (3)$$
$$C_2H_5Hg^+ \rightarrow \text{degradation products} \rightarrow Hg^{2+} \qquad k_{EtHg} \quad (4)$$
$$\text{2-MBA} \rightarrow \text{2-SBA} \qquad k_{MBA} \quad (5)$$
$$\text{2-SBA} \rightarrow UI \qquad k_{SBA} \quad (6)$$
$$UI \rightarrow \text{degradation products} \rightarrow SO_4^{2-} \qquad k_{UI} \quad (7)$$

The previous paper on the photocatalytic ethylmercury destruction [39] indicates that, after the formation of electron-hole pairs by TiO_2 irradiation (Eq. (8)), $C_2H_5Hg^+$ can be oxidized by $HO^\bullet$ or h_{VB}^+ (Eqs. (10) and (11)), or reduced by e_{CB}^- (Eq. (12)). Then, Hg(II), Hg(I) and Hg(0) can be formed; Hg(II) can be formed by $C_2H_5Hg^+$ oxidation (Eq. (10)), Hg(I) oxidation (Eq. (15)) or disproportionation (Eq. (18)). Hg(I) can be formed by Eqs. (11) and (19) followed by dimerization to Hg_2^{2+} (Eq. (12) (15)), or reduction to Hg(0) by e_{CB}^- (Eq. (19)) or even by an organic radical present in the system. It can be also oxidized to Hg(II) by e_{CB}^- injection into the TiO_2 conduction band (Eq. (17)). Hg(0) can be formed from Hg(I) (Eq. (20)) or by $C_2H_5Hg^\bullet$ dimerization (Eq. (14)), remaining over the TiO_2 surface, and in equilibrium with Hg_2^{2+} by reaction with Hg(II) (Eq. (19)). The proposed steps are the following:

$$TiO_2 + h\nu \rightarrow h_{VB}^+ + e_{CB}^- \quad (8)$$
$$H_2O + h_{VB}^+ \rightarrow HO^\bullet + H^+ \quad (9)$$
$$C_2H_5Hg^+ + h_{VB}^+/HO^\bullet \rightarrow C_2H_5^\bullet + Hg^{2+} (+ OH^-) \quad (10)$$
$$C_2H_5Hg^+ + h_{VB}^+/HO^\bullet \rightarrow C_2H_4Hg^{+\bullet} + H^+ (+ H_2O) \rightarrow C_2H_4 + Hg^+ \quad (11)$$
$$2\ Hg^+ \rightarrow Hg_2^{2+} \quad (12)$$
$$C_2H_5Hg^+ + e_{CB}^- \rightarrow C_2H_5Hg^\bullet \quad (13)$$
$$2\ C_2H_5Hg^\bullet \rightarrow (C_2H_5)_2Hg + Hg(0) \quad (14)$$
$$Hg^+ + O_2 \rightarrow Hg^{2+} + O_2^{\bullet-} \quad (15)$$
$$C_2H_5Hg^\bullet + H^+ + e_{CB}^- \rightarrow C_2H_6 + Hg(0) \quad (16)$$
$$Hg^+ \rightarrow Hg^{2+} + e_{CB}^- \quad (17)$$
$$Hg_2^{2+} \rightleftarrows Hg(0) + Hg(II) \quad (18)$$
$$Hg(II) + e_{CB}^- \rightarrow Hg(I) \quad (19)$$
$$Hg(I) + e_{CB}^- \rightarrow Hg(0) \quad (20)$$

In the case of TM, these reactions enhance TM removal and shift the equilibrium of complexation between $C_2H_5Hg^+$ with 2-MBA to the right. Anodic reactions lead to the formation of intermediates ($C_2H_5Hg^+$, 2-MBA, 2-SBA, UI, etc., expressed as RH) and to mineralization (Eq. (21)):

$$RH + h_{VB}^+ (HO^\bullet) \rightarrow \ldots \rightarrow CO_2 + H_2O \quad (21)$$

For example, for 2-SBA, mineralization would take place through Eq. (22):

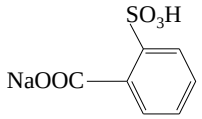

$$+ h_{VB}^+ (HO^\bullet) \rightarrow UI$$

$$\rightarrow \ldots CO_2 + H_2O + SO_4^{2-} \quad (22)$$

The already described heterogeneous photocatalytic treatment of C_2H_5HgCl [39] is faster than that of $C_2H_5Hg^+$ destruction formed during the photocatalysis of TM because 2-MBA and other derivatives may compete with the reaction of $C_2H_5Hg^+$ (Eq. (21)) for $h_{VB}^+/HO^\bullet$ and/or for the active sites over the TiO_2 surface.

Regarding SO_4^{2-}, it has been reported that TiO_2 has a good affinity for this anion [76] at acid pH, where the catalyst is positively charged. SO_4^{2-} reacts then with h_{VB}^+ or $HO^\bullet$ to yield the sulfate radical anion ($SO_4^{\bullet-}$), a very strong oxidant ($E^0 \approx$ 2.5 eV vs. SHE [77]), which enhances the mineralization. $SO_4^{\bullet-}$ can also react with e_{CB}^- or H_2O (Eqs. (23) to (26)). ([78, 79] and references therein).,

$$SO_4^{2-} + h_{VB}^+ \rightarrow SO_4^{\bullet-} \quad (23)$$
$$SO_4^{2-} + HO^\bullet \rightarrow SO_4^{\bullet-} + OH^- \quad (24)$$
$$SO_4^{\bullet-} + e_{CB}^- \rightarrow SO_4^{2-} \quad (25)$$
$$SO_4^{\bullet-} + H_2O \rightarrow HO^\bullet + SO_4^{2-} + H^+ \quad (26)$$

4.2. Kinetics

The temporal evolution of TM under N_2 was first fitted to the modified Langmuir-Hinshelwood model with three parameters adjusted to a hyperbolic deactivation, developed in the previous work for $C_2H_5Hg^+$ [39] and displayed in Eq. (S1) of section S2.1, together with a brief discussion. The

comparison with results of ref. [39] indicates that TM is more resistant to the photocatalytic treatment than $C_2H_5Hg^+$. With the reactor open to air, the rate constant for TM decay was 4 times higher than the value for the system under N_2; however, the fitting to this model under this condition was quite poor.

On the other hand, a simpler pseudo-first order decay was used to evaluate TM photocatalytic degradation. All equations are included in sections S2.2 and S2.3. In this case, the rate of the total TM decay to $C_2H_5Hg^+$ and 2-MBA was calculated with a very good fitting (R^2 = 0.990) for both systems (under N_2 and in air). The kinetic parameters and correlation coefficients of the results of Figs. 2, 3, and 4, corresponding to the temporal profiles of TM, $C_2H_5Hg^+$, 2-MBA, 2-SBA, and UI to these equations are in Table S1 of section S2.4. The comparison of both kinetic models (Eqs. (S1) and S3)) for TM degradation showed that the fitting was almost identical for TM under N_2, but that the fitting with Eq. (S3) was much better under air (see Fig. S2).

The kinetic constant k_{1TM} was obtained from Eq. (S3) by integrating Eq. (S2) [80]. In Eq. (S3), $[TM]_e$ is the TM concentration after the adsorption equilibrium was reached, and C represents the amount of TM that will be not degraded even after very long irradiation times; both TM values were fixed parameters for a given run, and were determined from the experimental data shown in Fig. 2. A possible reason for the good fitting is that TM adsorption equilibrium can be fast and, therefore, $[TM]_e$ is representative of adsorbed TM; this is especially possible because no deactivation of the photocatalyst seems to take place before TM has been completely degraded, either under N_2 or in air. Indeed, no significant Hg(0) deposition, appreciated by the change in the suspension color from pure white to gray, was observed up to 60 min, when TM degradation was ≈ 80% and almost 100% under N_2 or in air, respectively (see Figs. (2)-(4)). As the presence of O_2 inhibits Hg(0) deposition and thus, TiO_2 deactivation [29,33], this supports the fact that TM is degraded faster in the presence of O_2. On the other hand, this contrasts with other organomercurial compounds and suggests that the degradation takes place almost exclusively by the oxidative pathway. If the e_{CB}^- had contributed, the degradation rate would be smaller by the competence of O_2 with e_{CB}^-.

The fittings of the temporal evolution of $C_2H_5Hg^+$, 2-MBA, 2-SBA, and UI according to Eqs. (S6), (S7), (S9), and (S11) are displayed in Figs. 3 and 4, and the fitting parameters are shown in Table S1, with $[TM]_e$ and C having the same meaning as in Eq. (S3). The rather good fitting reinforces the fact that this consecutive first-order reaction model represents quite well the behavior of the system, according to the reaction scheme proposed in Eqs. (2) to (7) and is consistent with the experimental results. Table S1 also shows that the results are similar under N_2 and in air, with the exception of the rate constants, which are higher under air.

It is important to remember that, in a photocatalytic system, reactions are not strictly first-order, because, i.e., species involved in adsorption/desorption equilibria or charge transfer reactions may not attain steady-state concentrations. Therefore, pseudo-first order regimes should be considered, although the almost identical values obtained for k_{1MBA}, k_{1SBA}, and k_{1UI} in Table S1 under both N_2 and air supports the consecutive first order regime proposed. However, a deviation is clearly observed on the decay of TM, as k_{1TM} should be equal to the sum of k_{1EtHg} and k_{1MBA}; contrarily, k_{1TM} is always less than half the sum of k_{1EtHg} and k_{1MBA}, either under N_2 or in air. The parameter $[TM]_e$, representing the concentration of TM that is degraded either to $C_2H_5Hg^+$ or to 2-MBA, was calculated from Eqs. (S6) and (S7), respectively. In Table S1, it can be appreciated that the sum of $[TM]_e$ for $C_2H_5Hg^+$ and for 2-MBA is close to the initial TM concentration (≈ 0.5 mM). The parameters k_{1EtHg} and k_{1MBA} represent the time that the degradation pathway (Eqs. (2) and (3)) will contribute to TM degradation, with the smaller kinetic parameters contributing at longer times.

It should be remembered that the concentration of 2-MBA measured corresponds to a complex between 2-MBA and Hg^{2+} (or other Hg-containing compounds), otherwise $C_2H_5Hg^+$ and 2-MBA would rapidly recombine to generate TM. As said, no significant TM degradation was detected in control experiments in the dark, indicating that this enhanced decomposition of TM into $C_2H_5Hg^+$ + 2-MBA takes place only under irradiation.

Taking into account that k_{1TM} under N_2 is lower than the value under air (Table S1), this confirms that TM degradation takes place mainly by an oxidative mechanism initiated by h_{VB}^+/HO$^\bullet$, most probably because the first degradation step does not involve the reduction of the Hg-containing group. This contrasts with the degradation of other organomercurial compounds, such as CH_3Hg^+, $C_2H_5Hg^+$, or phenylmercury, which are degraded faster under N_2 atmosphere, indicating that both oxidative and reductive mechanisms take place simultaneously [5,35,39].

On the other hand, Fig. 4 shows that the fitting of $C_2H_5Hg^+$ deviates significantly from the consecutive pseudo-first order kinetics of formation and decay at $t \geq 60$ min; indeed, a better fitting of $C_2H_5Hg^+$ can be obtained using a combined pseudo-first order plus zero order decay for $t \geq 15$ min (green dashed lines). This can be rationalized considering that at t = 15 min, TM degradation is almost complete and, thus, $C_2H_5Hg^+$ formation is arrested. After this time, $C_2H_5Hg^+$ degradation continues by the pseudo-first order model; however, due to the TiO_2 deactivation and/or to the competition of other by-products, the degradation kinetics slows down in a more pronounced way than that expected from a pseudo-first order and continues instead by an almost zero order behavior, especially at $t \geq 60$ min.

It is important to point out that the amount of Hg in solution found at the end of the experiments is not low (1 mg L^{-1}, and 0.2 mg L^{-1}, under N_2 and air respectively). These values were obtained from TM + $C_2H_5Hg^+$ and the value of free Hg(II) is around 10 mg L^{-1} under both conditions. However, the value recommended by the WHO for inorganic Hg in drinking water (0.006 mg L^{-1} [23]) might be reached with longer reaction times or increasing the pH after the complete removal of $C_2H_5Hg^+$, as indicated in reference [39].

CONCLUSION

TiO_2-photocatalytic degradation is a suitable technique for the treatment of TM and its degradation products. In contrast to the treatment of ethyl- or phenylmercury salts reported in the previous articles of the group, and of methylmercury reported by others, the degradation of TM is faster in the presence of O_2.

The degradation kinetics of TM under N_2 or with the reactor open to air could be properly fitted to a pseudo-first order kinetics, together with the formation and degradation of the detected intermediates ($C_2H_5Hg^+$, 2-MBA, 2-SBA, and an aromatic unidentified intermediate). Mercury release from the organic structure is due to the attack of $HO^\bullet$ or h_{VB}^+. After 240 min of reaction, a significant TM mineralization (> 60%) could be obtained, for both NPOC and total S.

The photocatalytic reaction of 2-SBA is also efficient, and mineralization can be reached. However, TM proved to be more easily degraded than 2-SBA. Sulfate ions are the final product of all these reactions.

It has been suggested that Hg(0) can be transferred to the gas phase, becoming a new contaminant in air. To avoid this problem, the system can be coupled with a gas-phase photocatalytic reactor, which can efficiently remove Hg(0) [81] or using a Cu(0) powder filter that can retain 90% Hg(0) as amalgam [38]. This study will be undertaken in the future.

FUNDING

This work was supported by Agencia Nacional de Promoción Científica y Tecnológica (ANPCyT) from Argentina under PICT-2011-0463 and PICT-2015-0208 grants.

Supportive/Supplementary Material

A supporting information section (SI) is included as a separate file including: 1) the absorption spectrum of TM and 2) the kinetic equations for TM photocatalytic degradation and its degradation products.

Conflict of interests

The authors declare no conflict of interests for the publication of the present results.

REFERENCES

[1] D'Itri, F.M. *The Environmental Mercury problem*, Chem. Rubber Co., Cleveland, OH, **1972**.

[2] Kaiser, G.; Tölg, G. Mercury In: *Environmental Photochem.*; O. Hutzinger, Ed.; Springer, Berlin, **1960;** Vol. 3, Part A, pp. l–101.

[3] Ling, L.; Fan, M.; Wang, B.; Zhang, T. Application of computational chemistry in understanding the mechanisms of mercury removal technologies: a review. *Energy Environ. Sci.*, **2015**, *8*, 3109−3133.

[4] Nolan, E.M.; Lippard, S.J. Tools and Tactics for the Optical Detection of Mercuric Ion. *Chem. Rev.*, **2008**, *108*, 3443–3480.

[5] Serpone, N.; Borgarello, E.; Pelizzetti, E. Photoreduction and photodegradation of inorganic pollutants: II. Selective reduction and recovery of Au, Pt, Pd, Rh, Hg, and Pb In: *Photocatalysis and Environment*; Schiavello, M., Ed.; Kluwer Academic Publishers, Dordrecht, **1988**, pp. 527−565.

[6] Powell, H.M.; Jamieson, W.A. Merthiolate as a Germicide. *Am. J. Hyg.*, **1931**, *13*, 296−310.

[7] Geier, D.A.; Sykes, L.K.; Geier, M.R. A review of thimerosal (merthiolate) and its ethylmercury breakdown product: specific historical considerations regarding safety and effectiveness. J. Toxicol. Environ. Health, Part B, **2007**, *10*, 575–596,

[8] Clarkson, T.W. The three modern faces of mercury. *Environ. Health Persp.* (Suppl. 1), **2002**, *110*, 11–23.

[9] Velicu, M.; Fu, H.; Suri, R.P.S.; Woods, K. Use of adsorption process to remove organic mercury thimerosal from industrial process wastewater. *J. Hazard. Mater.* **2007**, *148*, 599−605.

[10] Yeh, J.-D.; Chen, S. Heavy Metallic and Organometallic Ions Scavenging Using Silica-Based Adsorbent Functionalized with Ligands Containing Sulfur and Nitrogen Elements. *J. Chin. Chem. Soc.* **2012**, *59*, 98–106.

[11] Yepsen, O.; Contreras, D.; Santander, P.; Yáñez, J.; Mansilla, H.D.; Amarasiriwardena, D. Photocatalytic degradation of thimerosal in human vaccine's residues and mercury speciation of degradation by-products, *Microchem. J.* **2015**, *121*, 41–47.

[12] Magos, L. Neurotoxic character of thimerosal and the allometric extrapolation of adult clearance half-time to infants. *J. Appl. Toxicol.* **2003**, *23*, 263–269.

[13] Clements, C.J.; Ball, L.K; Ball, R.; Pratt, D. Thiomersal in vaccines. *The Lancet*. **2000**, *355*, 1279–1280.

[14] Parker, S.K.; Schwartz, B.; Todd, J.; Pickering, L.K. Thimerosal-containing vaccines and autistic spectrum disorder: a critical review of published original data. *Pediatrics*, **2004**, *114*, 793–804 [Erratum in: Pediatrics 2005;115:200.]

[15] Bensefa-Colas, L., L'exposition précoce au thiomersal justifie les préoccupations lors de la discussion sur l'intoxication par le mercure: commentaire sur l'article de Bensefa-Colas et al., *La Revue de medecine interne*, **2012**, *33*, 115−116.

[16] Geier, D.A.; Geier, M.R. A Prospective Study of Mercury Toxicity Biomarkers in Autistic Spectrum Disorders. *J. Toxicol. Environ. Health, Part A: Current Issues*, **2007**, *70*, 1723–1730.

[17] Geier, D.A.; King, P.G.; Hooker, B.S.; Dórea, J.G.; Kerna, J.K.; Sykes, L.K.; Geier, M.R. Thimerosal: Clinical, epidemiologic and biochemical studies. *Clinica Chim. Acta*, **2015**, *444*, 212–220.

[18] Hornos Carneiro, M.F.; Oliveira Souza, J.M.; Grotto, D.; Lemos Batista, B.; de Oliveira Souza, V.C.; Barbosa, F. A systematic study of the disposition and metabolism of mercury species in mice after exposure to low levels of thimerosal (ethylmercury). *Environ. Res.*, **2014**, *134*, 218–227.

[19] Ida-Eto, M.; Oyabu, A.; Ohkawara, T.; Tashiro, Y.; Narita, N.; Narita, M. Embryonic exposure to thimerosal, an organomercury compound, causes abnormal early development of serotonergic neurons. *Neurosci. Lett.*, **2011**, *505*, 61– 64.

[20] Kern, J.K.; Geier, D.A.; Mehta, J.A.; Homme, K.G.; Geier, M.R. Mercury as a hapten: A review of the role of toxicant-induced brain autoantibodies in autism and possible treatment considerations. *J. Trace Elem. Med. Biol.*, **2020**, *62*, 126504.

[21] Kern, J.K.; Geier, D.A.; Homme, K.G.; Geier, M.R. Examining the evidence that ethylmercury crosses the blood-brain barrier. *Environ. Toxicol. Pharmacol.*, **2020**, *74*, 103312.

[22] Ramos, A.; dos Santos, M.M.; de Macedo, G.T.; Wildner, G.; Prestes, A.S.; Masuda, C.A.; Dalla Corte, C.L.; Teixeira da Rocha, J.B.; Barbosa, N.V, Methyl and Ethylmercury elicit oxidative stress and unbalance the antioxidant system in *Saccharomyces cerevisiae*, *Chemico-Biol. Interact.*, **2020**, *315*, 108867.

[23] WHO (World Health Organization),. Guidelines for Drinking-water Quality, 4th ed., WHO (ed.) Geneva, Switzerland, **2011**. Available at: http://whqlibdoc.who.int/publications/2011/9789241548151_eng.pdf. (Accessed 22/10/**2020**).

[24] Tan, M.; Parkin, J.E. Route of decomposition of thiomersal (thimerosal), *Int. J. Pharm.*, **2000**, *208*, 23−34.

[25] Fortunato, R.; Crespo, J.G.; Reis, M.A.M. Biodegradation of thiomersal containing effluents by a mercury resistant *Pseudomonas putida* strain. *Water Res.*, **2005**, *39*, 3511−3522.

[26] Gil, S.; Lavilla, I.; Bendicho, C. Greener analytical method for determination of thiomersal (sodium ethylmercury-thiosalicylate) in ophthalmic solutions using sono-induced cold vapour generation-atomic absorption spectrometry after UV/H_2O_2 advanced oxidation, *J. Anal. At. Spectrom.*, **2007**, *22*, 569–572.

[27] dos Santos, E.J.; Herrmann, A.B.; Bispo dos Santos, A.; Baika, L.M.; Sato, C.S.; Tormen, L.; Sturgeon, R.E.; Curtius, A.J. Determination of thimerosal in human and veterinarian vaccines by photochemical vapor generation coupled to ICP OES, *J. Anal. At. Spectrom.*, **2010**, *25*, 1627–1632.

[28] He, H.; Zhu, Z.; Zheng, H.; Xiao, Q.; Jin, L.; Hu, S. Dielectric barrier discharge micro-plasma emission source for the determination of thimerosal in vaccines by photochemical vapor generation, *Microchem. J.*, **2012**, *104*, 7–11.

[29] Botta, S.G.; Rodríguez, D.J.; Leyva, A.G.; Litter, M.I. Features of the transformation of HgII by heterogeneous photocatalysis over TiO_2. *Catal. Today*, **2002**, *76*, 247−258.

[30] Litter, M.I. Heterogeneous photocatalysis: transition metal ions in photocatalytic systems. *Appl. Catal. B: Environ.*, **1999**, *23*, 89–114.

[31] Litter, M.; Domènech, X.; Mansilla, H. Remoción de contaminantes metálicos In: *Eliminación de contaminantes por fotocatálisis heterogénea*. Blesa, M.A., Sánchez Cabrero, B. Eds.; Ediciones CIEMAT, Madrid, **2004**, pp. 163–187.

[32] Litter, M.I. Treatment of chromium, mercury, lead, uranium and arsenic in water by heterogeneous photocatalysis, *Adv. Chem. Eng.*, **2009**, *36*, 37–67.

[33] Litter, M.I.; Quici, N.; Meichtry, J.M.; Senn A.M. Photocatalytic removal of metallic and other inorganic pollutants In: *Photocatalysis: Applications*, Dionysiou, D.D.; Li Puma, G.; Ye, J.; Schneider, J.; Bahnemann, D. Eds.; Royal Society: London, **2016**, pp. 35−71.

[34] Quici, N.; Meichtry, J.M.; Montesinos, V.N, Photocatalytic Treatment of Inorganic Materials with TiO_2 Nanoparticles In: Encyclopedia of Nanoscience and Nanotechnology, Litter, M.I. Ed., American Scientific Publishers, Valencia, California, **2018**, Vol. 29, pp. 303–336.

[35] de la Fournière, E.M.; Leyva, A.G.; Gautier, E.A.; Litter, M. I. Treatment of phenylmercury salts by heterogeneous photocatalysis over TiO_2, *Chemosphere*, **2007**, *69*, 682–688.

[36] Miranda, C.; Yáñez, J..; Contreras, D; Zaror, C.; Mansilla, H.D. Phenylmercury degradation by heterogeneous photocatalysis assisted by UV-A light, *J. Environ. Sci. Health, Part A*, **2013**, *48*, 1642–648.

[37] Serpone, N.; Ah-You, Y.K.; Tran, T.P.; Harris, R. AM1 simulated sunlight photoreduction and elimination of Hg(II) and CH_3Hg(II) chloride salts from aqueous suspensions of titanium dioxide, *Solar Energy*, **1987**, *39*. 491–498.

[38] Miranda, C.; Yáñez, J..; Contreras, D; Garcia, R.; Jardim, W.F.: Mansilla, H.D. Photocatalytic removal of methylmercury assisted by UV-A irradiation, *Appl. Catal. B*, **2009**, *90*, 115–119.

[39] de la Fournière, E.M.; Meichtry, J.M.; Gautier, E.A.; Leyva, A.G.. Litter, M.I. Treatment of ethylmercury chloride by heterogeneous photocatalysis over TiO_2, *J. Photochem. Photobiol. A*, **2021**, *411*, 113205.

[40] Miranda-Andrades, J.R.; Khan, S.; Toloza, C.A.T.; Romani, E.C.; Freire Júnior, F.L.; Aucelio, R.Q. Thiomersal photo-degradation with visible light mediated by graphene quantum dots: Indirect quantification using optical multipath mercury cold-vapor absorption spectrophotometry, *Spectrochim. Acta B*, **2017**, *138*, 81–89.

[41] Herrmann, J.-M. Heterogeneous photocatalysis: fundamentals and applications to the removal of various types of aqueous pollutants, *Catal. Today*, **1999**, *53*, 115–129.

[42] Kerzhentsev, M.; Guillard, C.; Herrmann, J.-M.; Pichat, P. TiO_2-Photosensitised Degradation of Insecticide Tetrachlorvinphos ((z)-2-chloro-1(2,4,5-trichlorophenyl)ethenyl Dimethyl Phosphate In: *Photocatalytic, Purification and Treatment of Water and Air*, Ollis, D.F.; AI-Ekabi, H., Eds.; Elsevier Sci. Publish. B.V., Amsterdam, **1993**, pp. 601–606.

[43] Kerzhentsev, M.; Guillard, C.; Herrmann, J.-M.; Pichat, P. Photocatalytic pollutant removal in water at room temperature: case study of the total degradation of the insecticide fenitrothion (phosphorothioic acid O,O-dimethyl-O-(3-methyl-4-nitro-phenyl) ester), *Catal. Today*, **1996**, *27*, 215−220.

[44] Pelizzetti, E.; Maurino, V.; Minero, C.; Zerbinati, O.; Borgarello, E.. Photocatalytic degradation of bentazon by TiO_2 particles, *Chemosphere*, **1989**, *18*, 1437–1445.

[45] Hun, L.; Flanders, P.M.; Miller, P.L.; Strathmann, T.J. Oxidation of sulfamethoxazole and related antimicrobial agents by TiO_2 photocatalysis, *Water Res.*, **2007**, *41*, 2612–2626.

[46] Elmolla, E.S.; Chaudhuri, M. Photocatalytic degradation of amoxicillin, ampicillin and cloxacillin antibiotics in aqueous solution using UV/TiO_2 and UV/H_2O_2/TiO_2 photocatalysis, *Desalination*, **2010**, *252*, 46–52.

[47] Alfred, M.O.; Omorogie, M.O.; Bodede, O.; Moodley, R.; Ogunlaja, A.; Adeyemi, O.G.; Günter, C.; Taubert,

A.; Iermak, I.; Eckert, H.; Silva, I.D.A.; de Camargo, A.S.S.; Motheo, A.J.; Clarke, S.M.; Unuabonah, E.I.. Solar-active clay-TiO_2 nanocomposites prepared via biomass assisted synthesis: Efficient removal of ampicillin, sulfamethoxazole and artemether from water, *Chem. Eng. J.*, **2020**, *398*, 125544.

[48] Villegas-Guzman, P.; Silva-Agredo, J.; González-Gómez, D.; Giraldo Aguirre, A.L.; Flórez-Acosta, O.; Torres-Palma, R.A. Evaluation of water matrix effects, experimental parameters, and the degradation pathway during the TiO_2 photocatalytical treatment of the antibiotic dicloxacillin, *J. Environ. Sci. Health A*, **2015**, *50*, 40–48.

[49] Serna-Galvis, E.A.; Silva-Agredo, J.; Giraldo, A.L.; Flórez, O.A.; Torres-Palma, R. A.. Comparison of route, mechanism and extent of treatment for the degradation of a *β*–lactam antibiotic by TiO_2 photocatalysis, sonochemistry, electrochemistry and the photo-Fenton system, *Chem. Eng. J.*, **2016**, *284*, 953–962.

[50] Li, G.; Wang, B.; Xu, W.Q.; Han, Y.; Sun, Q. Rapid TiO_2/SBA-15 synthesis from ilmenite and use in photocatalytic degradation of dimethoate under simulated solar light, *Dyes and Pigments*, **2018**, *155*, 265–275.

[51] Bian, Z.; Feng, Y.; Li, H.; Yu, H.; Wu, H. Adsorption-photocatalytic degradation and kinetic of sodium isobutyl xanthate using the nitrogen and cerium co-doping TiO_2-coated activated carbon, *Chemosphere*, **2021**, *263*, 128254.

[52] Aboel-Magd A.; Abdel-Wahab; Gaber, A. El-A.M. TiO_2-photocatalytic oxidation of selected heterocyclic sulfur compounds, *J. Photochem. Photobiol. A*, **1998**, *114*, 213–218.

[53] Lin, F.; Zhang, Y.; Wang, L.; Zhang, Y.; Wang, D.; Yang, M.; Yang, J.; Zhang, B.; Jiang, Z., Li, C. Highly efficient photocatalytic oxidation of sulfur-containing organic compounds and dyes on TiO_2 with dual cocatalysts Pt and RuO_2, *Appl. Catal. A*, **2012**, *127*, 363–370.

[54] Ramacharyulu, P.V.R.K.; Kumar, J. P.; Prasad, G.K.; Sreedhar, B. Sulphur doped nano TiO_2: Synthesis, characterization and photocatalytic degradation of a toxic chemical in presence of sunlight, *Mat. Chem. Phys.*, **2014**, *148*, 692–698.

[55] Lin, Y.-H.; Hsueh, H.-T.; Chang, C.-W.; Chu, H. The visible light-driven photodegradation of dimethyl sulfide on S-doped TiO_2: characterization, kinetics, and reaction pathways, *Appl. Catal. B.*, **2016**, *199*, 1–10.

[56] Hitam, C.N.C.; Jalil, A.A.; Triwahyono, S.; Ahmad, A.; Jaafar, N.F.; Salamun, N.; Fatah, N.A.A.; Teh, L.P.; Khusnun, N.F.; Ghazali, Z. Synergistic interactions of Cu and N on surface altered amorphous TiO_2 nanoparticles for enhanced photocatalytic oxidative desulfurization of dibenzothiophene, *RSC Adv.*, **2016**, *6*, 76259–76268.

[57] Hitam, C.N.C.; Jalil, A.A.; Triwahyono, S.; Rahman, A.F.A.; Hassan, N.S; Khusnun, N.F.; Jamian, S.F.; Mamat, C.R.; Nabgan, W.; Ahmad, A.. Effect of carbon-interaction on structure-photoactivity of Cu doped amorphous TiO_2 catalysts for visible-light-oriented oxidative desulphurization of dibenzothiophene, *Fuel*, **2018**, *216*, 407–417.

[58] Poo-arporn, Y.; Kityakarn, S.; Niltharach, A.; Smith, M.F.; Seraphine, S.; Wörnerf, M.; Worayingyong, A. Photocatalytic oxidation of thiophene over cerium doped TiO_2 thin film, *Mat. Sci. Semicon. Proc.*, **2019**, *93*, 21–27.

[59] Sengele, A.; Robert, D.; Keller, N.; Colbeau-Justin, C.; Keller, V. Sn-doped and porogen-modified TiO_2 photocatalyst for solar light elimination of sulfure diethyle as a model for chemical warfare agent, *App. Catal. B*, **2019**, *245*, 279–289.

[60] Lu, X.; Li, X.; Qian, J.; Miao, N.; Yao, C.; Chen, Z. Synthesis and characterization of CeO_2/TiO_2 nanotube arrays and enhanced photocatalytic oxidative desulfurization performance, *J. Alloys Comp.*, **2016**, *661*, 363–371.

[61] Lu, X.; Li, X.; Chen, F.; Chen, Z.; Qian, J.; Zhang, Q. Biotemplating synthesis of N-doped two-dimensional CeO_2-TiO_2 nanosheets with enhanced visible light photocatalytic desulfurization performance, *J. Alloys Comp.*, **2020**, *815*, 152326.

[62] Xu, H.; Shi, J.-L.; Lyu, S.; Lang, X. Visible-light photocatalytic selective aerobic oxidation of thiols to disulfides on anatase TiO_2, *Chinese J. Catal.*, **2020**, *41*, 1468–1473.

[63] Cantau, C.; Larribau, S.; Pigot, T.; Simon, M.; Maurette, M.T.; Lacombe, S. Oxidation of nauseous sulfur compounds by photocatalysis or Photosensitization, *Catal. Today*, **2007**, *122*, 27−38.

[64] de la Fournière, E.M.; Litter, M.I.; Gautier, E.A.. Detection of mercury species by HPLC using 2-mercaptopropionic acid as complex agent, *J. Arg. Chem. Soc.*, **2013**, *100*, 1−8.

[65] Martí, F.B.; Conde, F.L.; Jimeno, S.A. *Química Analítica Cualitativa*, Paraninfo, Madrid, **1994**, p. 435.

[66] Tennakone, K.; Ketipearachchi, U.S. Photocatalytic method for removal of mercury from contaminated water, *Appl. Catal. B*, **1995**, *5*, 343–349.

[67] Kolthoff, I.M.; Sandell, E.B.; Meehan-Stanley Bruckenstein, E.J.. *Análisis Químico Cuantitativo*, Nigar, Buenos Aires, **1969**, p. 808.

[68] Tennakone, K.; Thaminimulle, C.T.K.; Senadeera, S.; Kumarasinghe, A.R. TiO_2-catalysed oxidative photodegradation of mercurochrome: an example of an organo-mercury compound, *J. Photochem. Photobiol. A*, **1993**, *70*, 193–195.

[69] Methods for the examination of water and associated materials In: Sulphate in Waters Effluents and Solids, Standing Committee of Analysis, HMSO, London, **1979**.

[70] Santos, J.C.N.; da Silva, I.M.; Braga, T.C.; de Fátima, A.; Figueiredo, I.M.; Santos, J.C.C. Thimerosal changes protein conformation and increase the rate of fibrillation in physiological conditions: Spectroscopic studies using bovine serum albumin (BSA), *Int. J. Biol. Macromol.*, **2018**, *113*, 1032–1040.

[71] López-Muñoz, M.J.; Arencibia, A.; Cerro, L.; Pascual, R.; Melgar, A. Adsorption of Hg(II) from aqueous solutions using TiO_2 and titanate nanotube adsorbents, *Appl. Surf. Sci*., **2016**, *367*, 91−100.

[72] Aguado, M.A.; Cervera-March, S.; Giménez, J. Continuous photocatalytic treatment of mercury(II) on

titania powders, Kinetics and catalyst activity, *Chem. Eng. Sci.*, **1995**, *50*, 1561−1569.

[73] Montesinos, N.; Salou, C.; Meichtry, J.M.; Colbeau-Justin, C.; Litter M.I. Role of Cr(III) deposition during the photocatalytic transformation of hexavalent chromium and citric acid over P25 and UV100, *Photochem. Photobiol. Sci.*, **2016**, *15*, 228–234);

[74] Ravichandran, M. Interactions between mercury and dissolved organic matter-a review. *Chemosphere*, **2004**, *55*, 319–331.

[75] Wu, X.; Liang, H.; O'Hara, K.A.; Yalowich, J.C.; Hasinoff, B.B. Thiol-Modulated Mechanisms of the Cytotoxicity of Thimerosal and Inhibition of DNA Topoisomerase IIr., *Chem. Res. Toxicol.*, **2008**, *21*, 483–493.

[76] Horányi, G. Investigation of the specific adsorption of sulfate ions on powdered TiO_2, *J. Colloid Interface Sci.*, **2003**, *261*, 580−583.

[77] Gau, B.C.; Chen, H.; Zhang, Y.; Gross, M.L. The Sulfate Radical Anion is a New Reagent for Fast Photochemical Oxidation of Proteins (FPOP), *Anal. Chem.*, **2010**, *82*, 7821–7827.

[78] Litter, M.I. Introduction to oxidative technologies of water treatment In: *Advanced Nano-Bio Technologies for Water and Soil Treatment*, Zbořil, R.; Černík, M.; Cajthaml, T.; Filip, J.; Najmanová, P. Eds., Springer, New York, **2020**, pp. 119−175.

[79] Wei, L.; Shifu, C.; Wei, Z.; Sujuan, Z. Titanium dioxide mediated photocatalytic degradation of methamidophos in aqueous phase, *J. Hazard. Mat.*, **2009**, *164*, 154–160.

[80] Bailey, R.C.; Eadie, G.S.; Schmidt, F.H. Estimation Procedures for Consecutive First Order Irreversible Reactions. *Biometrics*, **1974**, *30*, 67–75.

[81] Liu, D.; Li, B.; Wu, J.; Liu, Y. Photocatalytic oxidation removal of elemental mercury from flue gas. A review, *Environ. Chem. Lett.*, **2020**, *18*, 417–431.